Homogeneous Aerosol Formation by the Chlorine Atom Initiated Oxidation of Toluene

Rune S. Karlsson,† Joseph J. Szente, James C. Ball, and M. Matti Maricq*

Research Laboratory, Ford Motor Company, P.O. Box 2053, Drop 3083, Dearborn, Michigan 48121

Received: May 17, 2000; In Final Form: November 7, 2000

The photolysis of Cl_2 molecules in the presence of toluene and oxygen, at levels of $\sim 10^{14}$ radicals/cm^{-3}, initiates a sequence of chemical reactions that rapidly produce an aerosol. Size distributions of the aerosol particles are examined, using a scanning mobility particle sizer, as a function of time, photolysis energy, the initial concentrations of toluene and chlorine, and of added NO and HO_2. The number of particles and the volume of aerosol both exhibit a steep nonlinear increase as the initial chlorine atom level is raised. Surprisingly, the number of particles displays a strong inverse dependence on the initial toluene concentration, whereas the aerosol volume remains nearly unaffected by toluene level. Kinetic measurements of particle formation made using a flow reactor reveal an incubation period after initiation of the $Cl + C_6H_5CH_3$ reaction, followed by steep increases in particle number and volume. The particle number rapidly reaches a plateau, whereas the aerosol volume continues to increase with time. The earliest observed particles are unexpectedly large, with mean diameters as high as 100 nm; a continuous growth from <10 nm is generally not observed. Both NO and HO_2 suppress aerosol formation. These observations prompt us to postulate a mechanism whereby a minor reaction channel between chlorine atoms and benzylperoxy radicals to produce a Criegee intermediate controls the number of critical nuclei. This rate-limiting step is followed by rapid condensation of semivolatile compounds onto the nuclei. Because the aerosol volume can represent 10%, or more, of the toluene consumed, this necessarily includes products from the major oxidation pathways. As part of this work, we report 295 K rate constants of $k_4 = (8 \pm 2) \times 10^{-12}$ cm^3 s^{-1} for the benzylperoxy self-reaction, and $k_6 = (2.7 \pm 0.5) \times 10^{-11}$ cm^3 s^{-1} for its reaction with NO.

I. Introduction

Attention to the sources and fates of atmospheric particulate matter (PM) has surged in recent years following epidemiological findings that reveal a correlation between particle concentrations and adverse health effects.[1,2] Although the correlation is weak, and the toxicological mechanism remains unknown, there has been sufficient concern for the Environmental Protection Agency to reexamine the ambient particulate standard and to issue a new $PM_{2.5}$ standard for particles with aerodynamic diameters below a 2.5 μm cutpoint.[3] Source apportionment of PM is a daunting task, made difficult by the very wide range in chemical and physical properties of this atmospheric constituent. Differentiation of PM_{10} and $PM_{2.5}$ cutpoints mitigates this somewhat by distinguishing to a degree PM generated via mechanical, abrasive, processes, which produce primarily particles in the 1−10 μm diameter range, from those created chemically, which tend to be smaller than ~ 1 μm.

Despite this, understanding the origins of PM remains a complex issue. Even $PM_{2.5}$ particles are produced by a variety of anthropogenic and biogenic sources. To complicate matters, they arise from both primary and secondary origins. Soot from combustion sources, both stationary and mobile, is an example of a primary PM source, whereas sulfate and nitrate aerosols are major secondary constituents. Another secondary source, about which considerably less is known, is secondary organic aerosol (SOA). This class of particles is formed by the photochemically initiated oxidation of volatile organic compounds, under conditions similar to those leading to tropospheric ozone. The concentration of secondary aerosol varies widely with location and time. For example, during extreme smog episodes in the Los Angeles basin SOA may account for 70−75% of the total organic aerosol burden.[4−6] The precursors to SOA derive from both biogenic sources,[7] e.g., terpenes from conifer trees, and anthropogenic sources such as aromatic compounds[8] emitted from fossil fuel combustion.

The relative contribution of these sources to the overall PM burden remains an important issue. A good deal of work has gone into smog chamber studies[9,10] and model development[11−13] of the gas versus aerosol partitioning of organic vapors. Photochemical oxidation modifies the hydrocarbons that are emitted into the atmosphere, providing them with a variety of functional groups such as carbonyl, hydroxy, hydroperoxy, carboxylic acid, and others, many of which have very low vapor pressures and can condense onto nuclei, and others that may adsorb onto preexisting aerosol droplets.[14] The OH-initiated oxidation of aromatic compounds, including toluene, figures prominently in this regard. Seinfeld and co-workers have reported that it is the aromatic content of gasoline that determines its aerosol-forming potential.[15]

A principal aim of atmospheric aerosol chemistry is to characterize the quantities of semivolatile species produced from photochemical oxidation of anthropogenic and biogenic emissions, and to combine these data with thermodynamic properties in order to model the aerosol-forming potential of the emissions. The intent of the present work is somewhat different. It is to connect the gas phase chemistry that initiates the oxidation process, a subject that has received considerable attention, with the nature of the aerosol that is formed; that is, how are changes in the gas phase chemistry reflected in the aerosol character-

* Author for correspondence.
† Present address: TSI Inc., P.O. Box 64394, St. Paul, MN 55164.

10.1021/jp001831u CCC: $20.00
Published on Web 12/14/2000

istics? Thus, the experiments reported herein are not meant to represent atmospheric conditions. First, the initial radical concentrations are much higher than in the atmosphere. But the radicals are formed only during a very narrow time interval to initiate the chemistry, and not continually as in steady state smog chamber experiments; thus, the typical aerosol yield is actually less than in the latter experiments. Second, chlorine atoms, and not hydroxyl radicals, are used here to initiate the radical chemistry. Except in special circumstances, such as the possible role of halogen chemistry in ozone removal during the arctic sunrise,[16] Cl-initiated oxidation of hydrocarbons is of minor tropospheric importance. In fact, the supposedly simpler Cl reaction with toluene, which occurs via hydrogen abstraction from the methyl group, was not expected to yield an aerosol, since it is the ring-opening products from OH attack of the aromatic group that are attributed to aerosol formation.[17]

In this paper we present a kinetic and mechanistic examination of the Cl-initiated oxidation of toluene starting with the chemistry of the initial hydrocarbon radicals that are formed, and continuing with an exploration of the physical and chemical characteristics of the aerosol that is produced. Flash photolysis/time-resolved UV spectroscopy allows us to identify the benzylperoxy radical and observe its conversion to benzaldehyde (also benzyl alcohol). The dynamics of aerosol formation are explored by measurements of particle number, size, and volume as a function of time and initial reactant conditions. After a description of the experimental method in section II, the gas phase and aerosol data are presented in sections III and IV, respectively. A number of key observations presented in section IV motivate the aerosol mechanism that we subsequently propose in section V. One is that nuclei mode particles are not observed; rather there is an initial quiescent stage exhibiting no particles, after which there is a rapid rise in particle number, but these are already 20−100 nm in diameter when they first appear. A second observation concerns the role of toluene; raising the toluene level has the unanticipated effect of lowering particle number, yet leaving the aerosol volume largely unaffected. These observations suggest that separate chemical pathways are responsible for nucleation and particle growth; a minor channel is key to initiating formation of the critical nuclei, whereas the major oxidation pathways contribute the substantial portion of the aerosol volume. The observations supporting this mechanism, as well as the issues of coagulation and condensation are the subjects of section V.

II. Experimental Section

Three types of experiments to characterize aerosol formation by the chlorine-initiated oxidation of toluene are reported: (a) UV absorbance measurements to investigate the initial gas phase chemistry, (b) measurements of the aerosol particle size distributions, and (c) GC/mass spectrometric analysis of particulate matter collected on filters. These were carried out using two apparatuses. In one case, chlorine atoms are formed by flash photolysis; in the other they are generated at prescribed points along a continuous flow reactor. The UV absorbance measurements were conducted solely with the flash photolysis apparatus, whereas particle measurements were performed using both systems. The experimental details follow.

A. Flash Photolysis System. This system has been previously described with respect to our gas phase kinetics studies.[18−20] To initiate the chemistry, a 10 ns pulse of 351 nm light from an excimer laser (Lambda Physik LPX301) is used to dissociate a small fraction of molecular chlorine in a slowly flowing $Cl_2/C_6H_5CH_3/O_2/N_2$ gas mixture. The laser beam, depending on pulse energy (180−500 mJ) and on the amount of Cl_2 (0.1−0.5 Torr), creates chlorine atom concentrations ranging from $(1-14) \times 10^{14}$ cm^{-3} along a 1.5 cm diameter cylindrical volume traversing the center of a 3.5 cm diameter, 52.8 cm long, temperature controlled, fused silica reaction cell. The bulk gas flow velocity is typically 15 cm/s; thus, 3.5 s is required to replace the full volume of the cell with a new gas charge. Laser repetition rates of $\leq$0.2 Hz are used to avoid the photolysis of gaseous products or aerosol particles by successive laser pulses.

The photolyzed chlorine atoms rapidly attack toluene, almost entirely by hydrogen abstraction from the methyl group,[21] to produce benzyl radicals, which quickly add O_2 to form benzylperoxy radicals

$$Cl + C_6H_5CH_3 \rightarrow C_6H_5CH_2 + HCl \quad (1)$$

$$C_6H_5CH_2 + O_2 + M \rightarrow C_6H_5CH_2O_2 + M \quad (2)$$

Typically, with toluene and O_2 concentrations of ~1 and ~ 20 Torr, respectively, the peroxy radical formation occurs on the time scale of a few microseconds or less. The benzylperoxy concentration, which to first order is independent of toluene and O_2 concentrations at these levels, is determined optically via its UV absorption over the 220−340 nm range (the absorption cross section is calibrated against that of ethylperoxy[18]). Subsequently, the benzylperoxy radicals react among themselves, or with NO or HO_2 when these are added, on time scales of 10^{-4} s, and aerosol formation is observed on the 10^{-1} s time scale. The details of this chemistry are the subjects of sections III and IV. At times longer than about 50 ms, the reaction products initially created in the volume swept out by the laser beam begin to mix with the remainder of the gas volume (diffusion to the walls occurs with a time constant of ~800 ms), leading at long times to a factor of 5.4 dilution of these products relative to the initially created chlorine atom concentration.

Toluene was obtained from Aldrich with a purity of 99.5%. The Cl_2 was provided by Matheson as a 5% mixture in N_2. O_2 (99.8%) and N_2 (99.999%) were obtained from MI Airgas. Gas flows are regulated by Tylan/Millipore mass-flow controllers, except for the Cl_2, which is controlled by a needle valve. Toluene is introduced to the gas mixture by a syringe pump which delivers a controlled amount of liquid toluene into a flowing stream of nitrogen that is preheated to 100 °C in order to ensure that the toluene vaporizes prior to mixing with the O_2 and Cl_2. Typical concentrations used in the experiments are 0.3−3.0 Torr of toluene, 0.1−0.5 Torr of chlorine, and 24−530 Torr of oxygen, with nitrogen added to bring the total pressure to 760 Torr. All the experiments are performed at 295 K.

B. Time-Resolved UV Spectroscopy. The kinetics of the benzylperoxy chemistry is monitored using UV absorption spectra taken with 10 μs resolution at various times (10 μs to 100 ms) following initiation by the photolysis pulse. A deuterium lamp provides the broadband UV probe source. The probe light is collimated and counterpropagated along the axis of the flow cell, overlapping the volume swept out by the photolysis laser beam. After dispersion by a 0.32 m monochromator (Instruments SA, HR320) with a 147 groove/mm grating, it impinges a gated, intensified, diode array detector (Princeton Instruments, IPDA-700SB and ST1000 controller). Spectra are recorded at a resolution of 2 nm and wavelength calibration of the diode array is achieved with a low-pressure mercury lamp. The spectra are typically averaged over 500 laser flashes. They normally cover the range of 190−340 nm; however, due to absorption by toluene, the usable range in the present experiments is limited to wavelengths greater than ~220 nm.

A number of absorbing species relevant to Cl-initiated toluene oxidation contribute to the spectrum of the reaction mixture including benzylperoxy, HO_2, benzaldehyde, benzyl alcohol, and toluene. The absolute UV cross sections for the latter three, stable, species are measured by flowing a known quantity of each compound through the flow cell and recording the corresponding absorption spectrum. The HO_2 cross section is reported in ref 22. The benzylperoxy absorption cross section is measured in the present study via calibration against an ethylperoxy spectrum created under identical conditions of laser power and gas composition, except for replacing the toluene by ethane. The composition of UV absorbing species at a time t after photolysis is then determined by fitting the absorbance at that time to a superposition of the reference spectra, namely

$$\mathrm{Abs}(t) = \sum [x_i]_t \, \sigma(x_i) l \qquad (3)$$

where l represents the path length, σ the absorption cross section, and $[x_i]_t$ the concentration of the ith species at delay time t. To simplify the fitting procedure, benzaldehyde, benzyl alcohol, and a residual absorption at long times (>10 ms) that could not be accounted for by these two species are combined into a generic "products" category.

C. Particle Size Distributions. Particle number concentrations and their sizes are measured using a scanning mobility particle sizer (SMPS) (TSI, Inc., Model 3934). This is accomplished by sampling a small fraction of the gas mixture (0.3 L/min from a total flow of 8.8 L/min) as it exits the reaction cell. The sampled aerosol is brought to a Boltzmann charge equilibrium by passing it by a ^{85}Kr radioactive source, and then injected along the outer wall of a cylindrical classifier through which passes a 3.0 L/min flow of particle free sheath air. An electric field, placed across the outer wall and a central electrode along the axis of the classifier, draws the positively charged particles toward the axis of the classifier. Small aerosol particles with high electrical mobility move across rapidly and impact the axial electrode; large particles with low mobility exit the classifier along with the excess sheath air. Only a small fraction of particles within a narrow mobility range find their way through an exit aperture and are counted by a condensation particle counter (CPC, TSI Inc. model 3025). Upon scanning the applied voltage from 0 to 10 kV (at the 0.3 L/min sample and 3.0 L/min sheath gas flow rates), the distribution of particles in the 16−670 nm mobility diameter range is measured with a size resolution of about 5% (the 3025 counter records particles down to 3 nm, although diffusion losses in the classifier affect performance below about 10 nm).

It should be noted that the Cl_2 present in the gas mixture affects the performance of the CPC. The TSI model 3010 CPC is unusable because even small, <0.1 Torr, quantities of chlorine cause the counter to register an overflow count rate, perhaps due to Cl_2 and butanol reactions promoted by the metallic saturator. Cl_2 does not cause such artificial counts with the model 3025 CPC, which uses a felt saturator, but it does contribute to contaminating the pumps and counting optics internal to the CPC, potentially leading to unreliable measurements. We did not completely avoid this problem in some of the earlier experiments, and this is likely to be at least partly responsible for variations that appear in the absolute particle concentrations between some data sets in Table 3 below. However, within a set of measurements, the trends and relative changes in particle number and volume, e.g., as a function of initial chlorine atom or toluene concentrations, are found to be quite repeatable, as are the sizes of particles measured under a given set of experimental conditions.

The SMPS is normally used to monitor aerosols whose concentrations remain constant over the ∼2 min necessary to scan the size range. The current situation is somewhat different. The photolysis laser flashes at intervals ranging from 5 to 10 s, whereas the gas charge in the cell is removed over a 3.5 s period. Nearly 1 s is then required to reestablish the aerosol after the next laser pulse. Thus, there exist periods of about 1−6 s during the SMPS scan that the aerosol concentration decreases toward zero before being replenished to its nominal value. The mixing that occurs within the reaction cell damps these fluctuations. Averaging typically three distribution measurements further reduces the remaining undulations in the recorded size distributions. The particle concentrations are corrected by accounting for the duty cycle defined by the laser repetition rate relative to the gas replenishment rate. For laser repetition rates slow enough to allow complete gas exchanges between pulses, the corrected size distributions are independent of repetition rate. The size distributions are also corrected for the dilution of the irradiated volume into the total volume of the reaction cell (a factor of ∼5.4). The following aerosol characteristics are determined from the corrected data: total number concentration, (geometric) mean particle diameter, and the aerosol volume concentration.

D. Continuous Flow Reactor. The necessity of sampling the aerosol to measure its size distribution precludes an examination of its time evolution using the flash photolysis apparatus. To overcome this, a continuous flow reactor has been designed. It consists of a 165 cm long, 2.9 cm diameter quartz tube through which a $C_6H_5CH_3/Cl_2/O_2/N_2$ gas mixture flows. Chlorine atoms are continuously generated at a prescribed point along the reactor by directing UV light (λ > 300 nm, beam width ∼1 cm) from a 100 W Hg arc lamp transversely across the tube. A minimum of 30 cm is allowed to establish a steady gas flow before the Cl_2 photolysis occurs. The toluene oxidation initiated at this point continues until the gas mixture is sampled at a distance of 5−100 cm downstream from the lamp. At 1 atm pressure and a typical flow rate of 20 slpm (standard liters per minute), the flow velocity is approximately 50 cm/s; thus, the evolution of the aerosol can be examined over the 0.1−2 s time range. Based on the flow velocity and the 1 cm photolysis zone, the time resolution is ∼0.02 s. Although diffusion in the flow cell and sample line likely degrades this value somewhat, changes in the aerosol properties can be observed over the 0.1 s time scale.

As with the flash photolysis apparatus, dissociation of the Cl_2 rapidly generates benzylperoxy radicals via reactions 1 and 2. These reactions are complete well within the approximately 10 ms that the flowing reaction mixture is exposed to the ∼1 cm wide beam of the Hg lamp; thus, wavelengths below ∼300 nm are filtered out in order to minimize potential photochemistry of the peroxy radicals or their subsequent reaction products. The substitution of ethane for toluene, and the collection and analysis of the acetaldehyde and ethanol products from the flow reactor, provide an estimate that an initial radical concentration of $\sim 3 \times 10^{14}$ cm^{-3} is generated under typical flow conditions.

In the present experiments, the flow reactor operates at a Reynolds number of ∼1000, thus near the upper end of the laminar flow regime. Because chlorine atoms are photolyzed uniformly across the cross section of the flow reactor, mixing issues are of limited importance. The subsequent benzylperoxy chemistry leads to aerosol formation in the interim between the photolysis and sampling points. Wall losses of the aerosol are found to be minimal. The introduction, either near the axis or along the walls of the reactor, of an ammonium nitrate aerosol, with a mean particle diameter of ∼80 nm and a concentration

TABLE 1: Cl-Initiated Toluene Oxidation Mechanism (R = C_6H_5)

no.	reaction	k(295 K) ($cm^3\ s^{-1}$)	ref
	$Cl_2 + h\nu \rightarrow 2Cl$		
1	$RCH_3 + Cl \rightarrow HCl + RCH_2$	6.1×10^{-11}	21
2	$RCH_2 + O_2 + M \rightarrow RCH_2O_2 + M$	1.4×10^{-12}	25
	$RCH_2 + Cl \rightarrow RCH_2Cl$	2.0×10^{-10}	26
	$RCH_2 + Cl_2 \rightarrow RCH_2Cl + Cl$	1.3×10^{-12}	27
	$RCH_2 + RCH_2 \rightarrow RCH_2CH_2R$	4.1×10^{-12}	28
	$RCH_2 + RCH_2O_2 \rightarrow 2RCH_2O$	$<1 \times 10^{-10}$	
4	$RCH_2O_2 + RCH_2O_2 \rightarrow$ products	$k_4 = 7.7 \times 10^{-12}$	21
4a	$RCH_2O_2 + RCH_2O_2 \rightarrow 2RCH_2O + O_2$	$0.4k_4$	
4b	$RCH_2O_2 + RCH_2O_2 \rightarrow RCHO + RCH_2OH + O_2$	$0.4k_4$	
4c	$RCH_2O_2 + RCH_2O_2 \rightarrow RCH_2OOCH_2R + O_2$	$0.2k_4$	
12	$RCH_2O_2 + Cl \rightarrow$ products	$k_{12} = 1.5 \times 10^{-10}$	38[a]
12a	$RCH_2O_2 + Cl \rightarrow RCH_2O + ClO$	$<0.1k_{12}$	present work
12b	$RCH_2O_2 + Cl \rightarrow RCHOO + HCl$	$0.9k_{12}$	
5	$RCH_2O + O_2 \rightarrow RCHO + HO_2$	1×10^{-14}	29[a]
	$RCH_2O + RCH_2O \rightarrow RCH_2OOH_2CR$	1×10^{-11}	24, 30[a]
	$RCH_2O + RCH_2O \rightarrow RCHO + RCH_2OH$		
	$RCH_2O + RCH_2O_2 \rightarrow$ products	3×10^{-12}	31[a]
7	$RCH_2O_2 + HO_2 \rightarrow RCH_2OOH + O_2$	1.0×10^{-11}	21
	$HO_2 + HO_2 \rightarrow HOOH + O_2$	2.9×10^{-12}	29
	HO_2 Generation		
	$CH_3OH + Cl \rightarrow CH_2OH + HCl$	5.0×10^{-11}	29
	$CH_2OH + O_2 \rightarrow HO_2 + CH_2O$	9.1×10^{-12}	29
	$CH_2OH + Cl_2 \rightarrow ClCH_2OH + Cl$	2.7×10^{-11}	32
	$CH_2OH + CH_2OH \rightarrow$ products	1.5×10^{-11}	33
	$CH_2O + Cl \rightarrow HCO + HCl$	7.3×10^{-11}	29
	$HCO + O_2 \rightarrow HO_2 + CO$	5.6×10^{-12}	29
	NO Chemistry		
	$RCH_2 + NO \rightarrow$ products	9.5×10^{-12}	34
6	$RCH_2O_2 + NO \rightarrow RCH_2O + NO_2$	2.7×10^{-11}	present work
	$RCH_2O_2 + NO_2 \rightarrow RCH_2O_2NO_2$	9×10^{-12}	29[a]
	$RCH_2O + NO \rightarrow$ products	$k = 6 \times 10^{-11}$	29[a]
	$RCH_2O + NO \rightarrow RCH_2ONO$	$0.8 \times k$	
	$RCH_2O + NO \rightarrow RCHO + HNO$	$0.2 \times k$	
	$RCH_2O + NO_2 \rightarrow RCH_2ONO_2$	3×10^{-11}	29[a]

[a] Estimated by comparison to analogous ethylperoxy or methylperoxy rate constant.

of 2500 particles/cm^3 (which is typical of the aerosol photochemically initiated from toluene) undergoes less than a 10% loss over the 100 cm reactor length.

After the prescribed reaction distance, the gas mixture is sampled through a diluting nozzle in order to quench further aerosol chemistry or dynamics prior to analysis with the SMPS. The diluter consists of two concentric cylinders ending in a blunt nose cone. From this end, a small fraction of the aerosol (0.2−1.0 L/min) is pulled through a small orifice into the central tube, which is constructed of sintered stainless steel. Pressurized N_2, introduced into the outer annulus, enters through the sintered walls to dilute the sample. The total flow relative to the N_2 diluent flow, both controlled using Tylan/Millipore flow controllers, determines the dilution ratio, which can be varied from 0:1 to >50:1 (typically 40:1). A short, ∼35 cm, 0.64 cm diameter Tygon tube brings the diluted aerosol to the SMPS inlet. At the sample flow rate of 0.3 L/min, the transit time is 2 s, and the diffusive loss of 10 nm particles is 12%; for larger particles the loss becomes progressively smaller.[23] Tests using ammonium nitrate aerosols reveal a linear relationship, with a slope of 0.97 ± 0.02, between the calculated dilution factor and the measured reduction in aerosol (number and volume) concentration. The reported aerosol number and volume concentrations are corrected back to their concentrations in the flow reactor.

E. Particle Chemical Composition. Aerosol samples for chemical composition analysis are collected onto 2 μm Teflon filters (Gelman Scientific). In both systems, flash photolysis and continuous flow, the filters are located at the exits of the reaction vessels, in series with the exhaust pumps, and the aerosol is sampled without dilution. Comparison of SMPS measurements of particle concentration upstream versus downstream of the filters confirms their efficiency to be >98%. Typically, 20−900 μg of particulate material, depending on experimental conditions, is collected over a period of approximately 45 min (∼500 laser shots).

The aerosol mass is determined by comparing the pre- and postsampling filter masses. After weighing, the support ring around the filter is removed (it contains the preservative BHT) and the filter is immersed in 2 mL of methylene chloride and agitated in an ultrasonic bath for 3 min. 2 μL aliquots are injected into a Finnigan MAT GC/MS for chemical analysis. Secondary extractions with hexane or methanol yield about 3% additional material, and do not reveal any substantial new components.

In addition to the unknown samples, reference compounds corresponding to identified components in the aerosol, as well as surrogates for suspected components, are injected into the GC/MS in order to quantify the instrument response. The compounds benzaldehyde, benzyl alcohol, toluene, and benzyl chloride (formed in our experiments via the $C_6H_5CH_2 + Cl_2 \rightarrow C_6H_5CH_2Cl + Cl$ reaction) are identified by comparison against reference standards. Benzyl hydroperoxide and benzyl nitrite are tentatively identified via their mass spectra. Additional reference compounds used to help identify and quantify the aerosol composition include *p*-chlorotoluene, *p*-creosol, *p*-nitrotoluene, dibenzyl, benzyl ether, and benzyl benzoate. On a relative 0−10 scale, the GC response to these compounds varies between 4.9 and 8.2, suggesting that the instrument sensitivity to the various toluene oxidation products that are

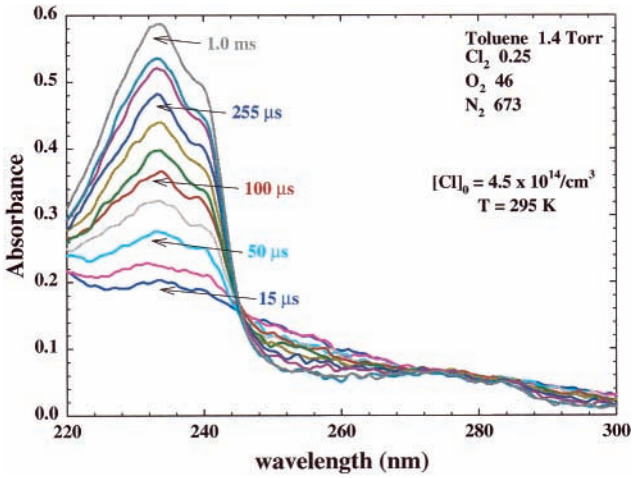

Figure 1. Time-resolved UV absorbance spectra after flash photolysis of a $Cl_2/C_6H_5CH_3/O_2/N_2$ reaction mixture.

observed, but not identified, varies less than ~40%. Control experiments, in which gaseous toluene, benzaldehyde, and benzyl alcohol are flowed at concentrations relevant to the current experimental conditions, reveal that these compounds are not collected from the gas phase by the filter; thus, their identification from the filter samples implies that they are found in the aerosol phase.

III. Results: Gas Phase Chemistry

Since aerosol formation is initiated by the chemical attack of toluene by chlorine atoms, it behooves us to describe briefly the principal features of the underlying gas phase chemistry (the reaction model is listed in Table 1). A limited amount of data is presented here: rate constant measurements for the benzylperoxy self-reaction rate are provided that confirm the single previously reported value, and new measurements of the rate constant for the benzylperoxy reaction with NO are given. These are not meant to represent a definitive study of these reactions, which would take us too far afield from the present objective, but they help provide a foundation for the gas phase chemistry that accompanies, and leads to, particle formation.

A. Peroxy Radical Chemistry. Chlorine atoms formed in the presence of toluene and oxygen by flash photolysis rapidly convert, via reactions 1 and 2, a fraction of the toluene molecules in the gas mixture (on the order of 10^{14} cm^{-3}) to benzylperoxy radicals. The principal fate of the peroxy radicals, in the absence of other reaction partners such as NO, or HO_2 , is to undergo self-reaction; thus

$$C_6H_5CH_2O_2 + C_6H_5CH_2O_2 \rightarrow 2C_6H_5CH_2O + O_2 \quad (4a)$$

$$\rightarrow C_6H_5CHO + C_6H_5CH_2OH + O_2 \quad (4b)$$

$$\rightarrow C_6H_5CH_2OOCH_2C_6H_5 + O_2 \quad (4c)$$

The branching fractions for channels 4a, 4b, and 4c are 40%, 40%, and 20%, respectively.[21] Only channel 4a propagates radicals, whereas the other two channels lead to stable molecular products.

Figure 1 illustrates the effect of the oxidation chemistry on the UV spectrum of the reaction mixture. An initially modest, broad, absorption over the 220−300 nm region grows to a narrower and more intense feature centered about 230 nm. The former belongs to the benzylperoxy radical, and the latter to

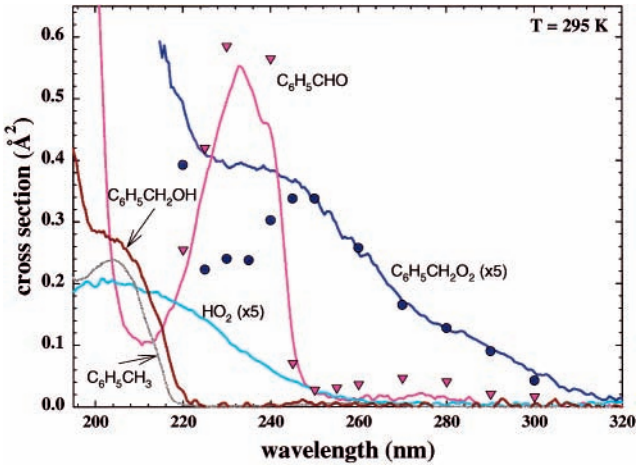

Figure 2. Reference spectra of the principal species contributing to the UV absorbances: benzylperoxy, benzaldehyde, hydroperoxy, benzyl alcohol, and toluene. Lines represent the present measurements; symbols represent the data from ref 21: circles $C_6H_5CH_2O_2$ and inverted triangles C_6H_5CHO.

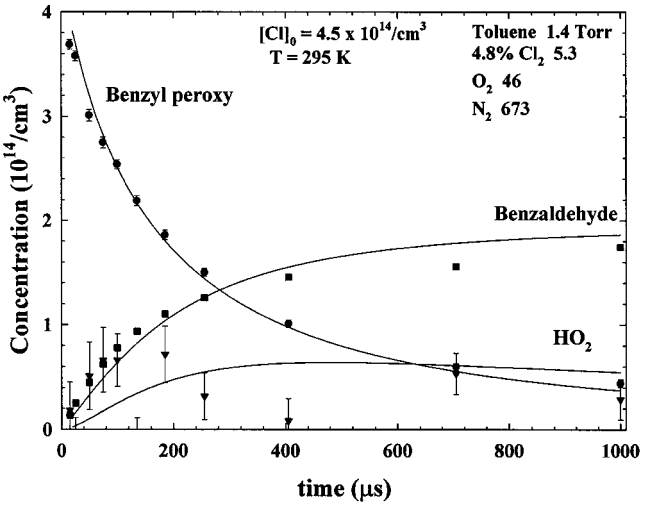

Figure 3. Concentration versus time profiles of benzylperoxy, benzaldehyde, and HO_2 following the self-reaction of benzylperoxy. Symbols represent concentrations deconvoluted from time-resolved UV spectra; lines represent calculations based on the reaction model of Table 1.

the benzaldehyde product formed in reaction 4b. Benzyl alcohol also exhibits a UV absorption at ~210 nm (Figure 2), but it is weaker and is buried under the toluene absorption that in the present experiments limits the UV range to >210 nm. The alkoxy radicals produced by reaction 4a can react with each other to form predominantly benzaldehyde and benzyl alcohol,[24] with benzylperoxy radicals to produce stable products, or they can react with molecular oxygen

$$C_6H_5CH_2O + O_2 \rightarrow C_6H_5CHO + HO_2 \quad (5)$$

to form hydroperoxy radicals and additional benzaldehyde. HO_2 exhibits a broad absorption band at 208 nm and, thus, contributes to a small extent to the absorbance at the short-wavelength side of Figure 1. It reacts with benzylperoxy radicals to form $C_6H_5CH_2OOH$, or with itself to produce HOOH.

Comparison of the UV absorbances taken at various times after photolysis to reference spectra, such as those depicted in Figure 2, provides a means to extract, via (eq 3), concentration versus time profiles for the UV-absorbing species. Figure 3 illustrates the benzylperoxy, benzaldehyde, and HO_2 concentra-

TABLE 2: $C_6H_5CH_2O_2$ Reaction Rate Constant Measurements

reaction partner	toluene (Torr)	Cl_2 (Torr)	O_2 (Torr)	NO (Torr)	$[Cl]_0$ (10^{14} cm^{-3})	k^a (10^{-12} cm^3/s)
$C_6H_5CH_2O_2$	1.4	0.25	46		4.6	7.6 ± 1.2
	0.73	0.14	46		1.6	9 ± 3
	0.3	0.24	47		4.3	6 ± 3
NO	1.5	0.23	49	0.025	4.32	33 ± 5
	1.5	0.24	48	0.051	4.48	25 ± 7
	1.5	0.23	48	0.099	4.34	23 ± 5

[a] Error bars are $\pm 2\sigma$ and include fitting and systematic uncertainties.

tions versus time as deconvoluted from the UV data, and compares them to the best fit predictions from the reaction model listed in Table 1, treating k_4 as an adjustable parameter (the scatter in the HO_2 data arises from the difficulty in deconvoluting its absorption from the stronger overlapping benzaldehyde and benzyl alcohol spectral features − Figure 2). Three rate constant determinations, utilizing different toluene concentrations, are listed in Table 2. The listed errors are 95% confidence limits that arise primarily from the noise associated with the UV absorbances, but also include a 10% systematic uncertainty in the benzylperoxy UV cross section. The weighted average yields a rate constant of $k_4 = (8 \pm 2) \times 10^{-12}$ cm^3 s^{-1}, which is in excellent agreement with the previously reported value[21] of $(7.0 \pm 1.6) \times 10^{-12}$ cm^3 s^{-1}.

The major products from the Cl initiated oxidation of toluene, using typical initial conditions of $[Cl]_0 = 4 \times 10^{14}$ cm^{-3} and $[C_6H_5CH_3]_0 = 4.9 \times 10^{16}$ cm^{-3}, are predicted by the model of Table 1 to be benzaldehyde, 1.8; benzyl alcohol, 0.64; dibenzyl peroxide, 0.33; and benzylhydroperoxide, 0.72, all in terms of 10^{14} molecules/cm^3. Together, these account for about 96% of the chlorine atoms generated by photolysis. The minor channels listed in Table 1 account for the remaining ~4%.

B. NO and HO_2 Chemistry. NO typically reacts rapidly with peroxy radicals; thus, its presence can radically alter the products produced from the toluene oxidation. The reaction

$$C_6H_5CH_2O_2 + NO \rightarrow C_6H_5CH_2O + NO_2 \qquad (6)$$

converts the peroxy radical to the corresponding alkoxy radical, producing NO_2 in the process. In effect, the added NO eliminates the molecular products formed from the self-reaction. The alkoxy radical then experiences a competition between reacting with NO to form benzyl nitrite, or with O_2 to form benzaldehyde and HO_2. The net result has a dramatic effect on the oxidation products; thus, ignoring the minor reactions with the NO_2 produced from reaction 6, the addition of 0.1 Torr of NO to the example above changes the product distribution to 1.0×10^{14} benzaldehyde/cm^3 and 2.5×10^{14} benzyl nitrite/cm^3. It also leads to a roughly 4-fold reduction in particle number.

Rate constants for the $C_6H_5CH_2O_2$ + NO reaction have not been previously reported. It is measured at 295 K as part of the present work using the time-resolved UV method described above for the peroxy self-reaction measurements. The results are reported in Table 2, including 95% confidence limits that include both signal noise and uncertainty in the UV cross sections. Taking the average of the measurements gives $k_6 = (2.7 \pm 0.5) \times 10^{-11}$ cm^3 s^{-1}. This value is on the high side of peroxy + NO rate constants, which typically range from $(0.5-2) \times 10^{-11}$ cm^3 s^{-1}.[35]

Although HO_2 is generated as a secondary intermediate originating from the self-reaction of benzylperoxy radicals, added HO_2 can also dramatically affect the nature of the oxidation products. In the present experiments, it is generated by chlorine attack of methanol that is added along with toluene to the gas mixture (see Table 1). The principal effect of introducing HO_2 at the beginning of the reaction sequence is to increase the yield of benzyl hydroperoxide, from the reaction

$$C_6H_5CH_2O_2 + HO_2 \rightarrow C_6H_5CH_2OOH + O_2 \qquad (7)$$

relative to those of benzaldehyde and benzyl alcohol. Thus, again using the example given above and adding 0.8 Torr of CH_3OH changes the product distribution to benzaldehyde, 1.0; benzyl alcohol, 0.33; dibenzyl peroxide, 0.17; and benzyl hydroperoxide, 1.0, all in terms of 10^{14} molecules/cm^3. The $HO_2 + C_6H_5CH_2O_2$ rate constant has been previously reported[21] as $(1.0 \pm 0.2) \times 10^{-11}$ cm^3 s^{-1}, and is not remeasured here.

IV. Results: Aerosol Formation

We turn now to examine the characteristics of the aerosol that is produced from the toluene oxidation. To gain an understanding into the process of particle formation, we investigate how particle number, size, and volume change as experimentally accessible parameters such as reactant concentrations and time are varied. A discussion of the implications of these results regarding the mechanism of aerosol formation is postponed to section V.

A. Dependence on $[Cl]_0$. In the absence of molecular chlorine, toluene, or the UV pulse to initiate oxidation, no particles are formed. When all three are present, increasing either the chlorine concentration or the laser intensity leads to a nonlinear increase in the number of particles formed, as illustrated in Figure 4. The increase in particle yield does not depend on whether $[Cl_2]_0$ or the laser pulse energy is increased; doubling either leads to approximately the same increase in particle number. This indicates that neither molecular chlorine nor laser power per se are involved in particle formation, for example eliminating the possibility that the photolysis laser weakly photoionizes the reaction mixture, and thereby generates nucleation sites for particle formation.

Instead, the Cl_2 concentration and photolysis light intensity play indirect roles, affecting the aerosol level via the initial chlorine atom concentration that is generated. Figure 5, provides a more detailed look at how the aerosol depends on the initial radical concentration (a complete list of the experimental results is provided in Tables 3 and 4). Measurements made using both the flash photolysis and continuous flow reactor systems show a 4 orders of magnitude increase in particle number concentration as $[Cl]_0$ is increased from $(1-14) \times 10^{14}$ cm^{-3}, with a very steep increase at low $[Cl]_0$ that subsequently flattens out. The aerosol volume exhibits a less dramatic increase with initial chlorine atom level because the average particle diameter decreases from about 150 to 50 nm. At low $[Cl]_0$ particle number grows roughly as $[Cl]_0^5$, whereas particle volume exhibits a more nearly $[Cl]_0^3$ dependence. At the higher end of the $[Cl]_0$ range these reduce to fourth- and second-order dependences, respectively, the number being limited by particle coagulation, and the volume being limited by the time and material available for particle growth. Assuming the generic "toluene oxidation product" to have a molecular weight of 100 amu and a density of 1.0 g/cm^3, the aerosol phase represents approximately 10% of the total product volume, as illustrated in the lower panel of Figure 5.

The flow reactor data in Figure 6 illustrate the role that time plays in aerosol development. At low initial chlorine atom levels ($[Cl_2]_0 = 1.3 \times 10^{16}$ cm^{-3}, or $[Cl]_0 \cong 1 \times 10^{14}$ cm^{-3}) there is a ~0.6 s incubation time after which particles appear at a rate

TABLE 3: Aerosol Measurements: Flash Photolysis

	experimental conditions (Torr)						SMPS measurements		
variable	$[Cl]_0$ ($\times 10^{14}$/cm^3)	toluene	$[Cl_2]$	$[O_2]$	$[CH_3OH]$	[NO]	particle no. ($\times 10^6$/cm^3)	particle volume ($\times 10^{11}$ nm^3/cm^3)	mean dia (nm)
$[Cl]_0$	1.3	1.5	0.12	47			0.01	0.14	76.7
	2.2	1.5	0.12	47			0.27	9.7	155.5
	2.6	1.5	0.25	47			1.1	12.4	89.5
	3.7	1.5	0.12	46			9.9	58.8	81.6
	4.6	1.5	0.25	46			17	55.8	65.1
	4.8	1.5	0.46	46			17	42.0	59.5
	8.0	1.5	0.25	46			83	144	54.9
	8.4	1.5	0.46	46			76	128	54.6
	14	1.5	0.46	46			151	305	58.7
$[O_2]$	4.3	1.5	0.24	24			7.1	28	70.7
	4.3	1.5	0.24	47			8.7	29	66.9
	4.3	1.5	0.24	95			9.7	26	63.1
	4.3	1.5	0.22	53			5.2	24	67.2
	4.3	1.5	0.22	530			7.6	16	55.7
[toluene]	1.6	0.031	0.24	49			16	3.7	29.3
	1.6	0.062	0.24	49			20	9.3	37.4
	1.6	0.12	0.24	49			19	13.7	42.0
	1.6	0.16	0.24	49			21	17.3	42.9
	1.6	0.22	0.24	49			16	17.7	47.3
	1.6	0.31	0.24	49			12	19.8	53.4
	1.6	0.62	0.24	49			4	24.1	76.6
	1.6	1.3	0.24	49			0.68	16.0	113.6
	1.6	1.6	0.24	49			1.5	26.9	110.8
	1.6	3.1	0.24	49			0.25	9.6	90.5
	1.6	0.030	0.21	47			3.1	0.75	30.6
	1.6	0.060	0.19	47			1.8	0.36	27.6
	1.6	0.30	0.19	47			1.3	2.0	55.0
	1.6	1.5	0.19	47			0.04	0.88	120.3
	1.6	2.2	0.19	47			0.01	0.45	103.6
	3.1	0.030	0.21	47			8.0	2.2	31.1
	3.1	0.060	0.19	47			7.8	2.9	33.7
	3.1	0.30	0.19	47			7.3	6.7	43.8
	3.1	1.5	0.19	47			1.1	12.2	95.3
	3.1	2.2	0.19	47			0.27	9.0	137.8
	5.5	0.030	0.21	47			14.2	5.9	34.2
	5.5	0.060	0.19	47			12.7	6.7	36.8
	5.5	0.30	0.19	47			13.9	15.7	45.5
	5.5	1.5	0.19	47			8.0	36	65.6
	5.5	2.2	0.19	47			4.6	39	78.8
	4.3	0.31	0.24	47			24.5	11.3	38.6
	4.3	0.77	0.24	47			12.8	13.1	47.6
	4.3	1.5	0.24	47			4.4	14.4	66.9
	4.3	2.4	0.24	47			1.8	14.3	88.5
	4.3	3.1	0.24	47			1.1	14.1	102.6
HO_2	3.8	1.55	0.23	49	0		2.8	26	84.3
	3.8	1.47	0.22	48	0		5.2	44	82.3
	4.7	1.55	0.23	49	0.41		0.75	19	124.4
	5.5	1.47	0.22	48	0.77		0.45	25	166.3
	5.5	1.55	0.23	49	0.81		0.11	9.5	184.6
	6.7	1.55	0.23	49	1.6		0.02	1.2	140.2
NO	3.8	1.55	0.24	48		0	11.8	79	81.3
	3.8	1.55	0.24	48		0.25	0.04	0.18	66.6
	3.8	1.55	0.24	48		0.19	0.27	1.09	69.6
	3.8	1.55	0.24	48		0.13	1.63	5.5	68.3
	3.8	1.55	0.24	48		0.08	6.0	15.2	64.6
	3.8	1.55	0.24	48		0.03	10.1	31	68.7
	3.8	1.55	0.24	48		0.02	5.6	34	85.3
	3.8	1.55	0.24	48		0	19.2	76	68.0
	4.0	1.6	0.25	49		0.40	0.0008	0.004	42.8
	4.0	1.6	0.25	49		0.34	0.002	0.01	47.6
	4.0	1.6	0.25	49		0.31	0.01	0.03	58.1
	4.0	1.6	0.25	49		0.28	0.02	0.07	61.7
	4.0	1.6	0.25	49		0.25	0.03	0.10	59.6
	4.0	1.6	0.25	49		0.20	0.16	0.75	71.5
	4.0	1.6	0.25	49		0.15	0.62	2.1	67.9
	4.0	1.6	0.25	49		0.10	1.63	4.4	62.9
	4.0	1.6	0.25	49		0.06	4.0	8.6	57.9
	4.0	1.6	0.25	49		0.02	2.5	12.9	77.9
	4.0	1.6	0.25	49		0.00	5.0	29	71.0
	4.2	1.54	0.24	47		0.49	0.02	0.05	64.0
	4.2	1.54	0.24	47		0.24	0.14	0.54	67.5
	4.2	1.54	0.24	47		0.24	0.03	0.63	54.2
	4.2	1.54	0.24	47		0.11	1.9	3.8	59.5
	4.2	1.54	0.24	47		0.11	1.5	3.1	62.0
	4.2	1.54	0.24	47		0.00	5.4	22.6	72.8
	4.2	1.54	0.24	47		0.00	8.8	27.5	68.8
	4.2	1.54	0.24	47		0.00	8.7	28.9	66.9

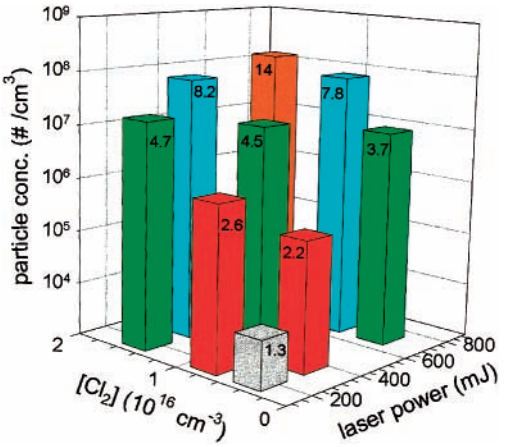

Figure 4. Aerosol particle number as a function of laser pulse energy and initial Cl_2 concentration. The numbers imprinted on each bar represent $[Cl]_0$ in units of 10^{14} cm^{-3}.

of $\sim 5 \times 10^4$ cm^{-3} s^{-1}, but only a relatively few are formed. As $[Cl]_0$ is increased, the incubation time decreases and progressively higher particle number concentrations are produced. At $[Cl_2]_0 = 5.2 \times 10^{16}$ cm^{-3} ($[Cl]_0 \cong 5 \times 10^{14}$ cm^{-3}) the incubation time shrinks to $\sim$0.1 s and the particle formation rate increases to $\sim 2 \times 10^7$ cm^{-3} s^{-1}. Aerosol volume follows qualitatively the same trends with respect to time and initial chlorine concentration. This behavior is consistent with the Cl-initiated toluene oxidation yielding semivolatile species that subsequently nucleate. Higher Cl levels imply faster formation and greater quantities of the semivolatile compounds and, thus, lead to higher nucleation rates.

Interestingly, there is an inverse correlation between particle size and $[Cl]_0$. The mean diameter of about 80 nm observed for the earliest particles under conditions of low $[Cl]_0$ shrinks to approximately 50 nm at the upper end of the $[Cl]_0$ range. At low $[Cl]_0$ the particles exhibit a slower secondary growth to about 120 nm over a period of about 1.5 s, presumably from the uptake of gaseous reaction products, whereas when $[Cl]_0$ is high no secondary growth is observed (the data in Figure 6 show a slight decrease in mean size, whereas a second similar dataset reveals the contour lines near 60 nm to be nearly horizontal). A more detailed discussion of the aerosol dynamics is postponed until the effects of toluene, oxygen, NO, and HO_2 on aerosol formation have been presented.

B. Dependence on Initial Toluene Concentration. According to the reaction model in Table 1, the amount of toluene initially present in the gas mixture should have little effect on the overall reaction kinetics or the product distribution. The toluene serves simply as a precursor for benzylperoxy radicals. With the typically employed quantities of $\sim$1 Torr of toluene and 50 Torr of O_2 , the photolyzed chlorine atoms are converted by reaction 1 to benzyl radicals in <1 μs and subsequently via reaction 2 to benzylperoxy radicals in another <1 μs. Thus, the high sensitivity of particle number density on the initial toluene concentration, displayed in Figure 7 and in Tables 3 and 4, is unexpected. That the toluene and particle number concentrations are inversely related, whereas the aerosol volume remains nearly unaffected, is even more surprising.

In Figure 7, the number concentration of particles decreases nearly exponentially as $[C_6H_5CH_3]_0$ is raised ($N \cong 7.8 \times 10^7$ exp(-0.62×10^{-16} $[C_6H_5CH_3]_0$) particles/cm^3 and $N \cong 1.8 \times 10^7$ exp(-0.48×10^{-16} $[C_6H_5CH_3]_0$) particles/cm^3, respectively, for the flow reactor and flash photolysis data). In contrast, the aerosol volume is almost independent of toluene level. Only at very low $[C_6H_5CH_3]_0$, where the photolyzed chlorine atoms are lost by recombination or to the walls of the reaction vessel, is a decrease in aerosol volume noted, and even here the dependence is much more muted as compared to number concentration. The lack of change in aerosol volume arises because of a nearly exponential increase in particle diameter with increasing $[C_6H_5CH_3]_0$ that effectively cancels the loss in particle number density. Again, the aerosol phase represents nearly 10% of the toluene oxidation products.

Figures 8 and 9 portray the combined influences of time and toluene level on the aerosol dynamics. The former figure illustrates the evolution of the number-weighted particle size distribution for toluene concentrations differing by a factor of 10. As indicated in the previous section, the evolution can be divided into three periods: First, there is an incubation period (of about 0.5 s at the high $[C_6H_5CH_3]_0$ and <0.2 s at low $[C_6H_5CH_3]_0$) during which no aerosol formation is observed. Second, there appears over the next 0.8 s a steep increase in particle number concentration (the rate decreases from $\sim 10^8$ cm^{-3} s^{-1} at $[C_6H_5CH_3]_0 = 4.3 \times 10^{15}$ cm^{-3} to $\sim 10^6$ cm^{-3} s^{-1} at $[C_6H_5CH_3]_0 = 8.6 \times 10^{16}$ cm^{-3}). Third, the particle number reaches a plateau, but the distribution shifts to larger size, with the mean particle diameter growing from $\sim$25 to $\sim$30 nm during the interval of 0.8$-$2.0 s at the low $[C_6H_5CH_3]_0$ and from $\sim$75 to $\sim$95 nm during the interval of 1.3$-$2.0 s at the high $[C_6H_5CH_3]_0$. It is surprising that the data give the appearance that the particles are born "nearly full grown". At the low initial toluene conditions, 20 nm particles are clearly evident, and the mean diameter only grows to $\sim$30 nm. In contrast, the mean particle diameter at the high toluene level is already at $\sim$70 nm at the time that the particles are first observed. This is not the expected aerosol evolution, in which a large number of very small particles, <20 nm, are initially formed and coagulate to produce a progressively smaller number of successively larger particles as time progresses.

Figure 9 amplifies the contrast between the evolutions of particle number versus aerosol volume. Except for the incubation period and initial sharp rise in particle number, the dependencies of particle number on time and $[C_6H_5CH_3]_0$ are nearly orthogonal to those of aerosol volume. Particle number reaches a plateau constant in time, the height of which is dictated by $[C_6H_5CH_3]_0$. In contrast, aerosol volume increases with time, but in comparison to particle number it is nearly independent of $[C_6H_5CH_3]_0$. As stated above, the different behaviors of particle number and volume evolutions remain consistent because of the nearly 3-fold increase in particle size as the toluene concentration is raised from $(1-8) \times 10^{16}$ cm^{-3}.

C. Dependence on O_2. As seen from the results in Table 3, the O_2 level has at best a minor impact on the aerosol characteristics. An increase in O_2 concentration by a factor of 20 affects particle number and aerosol volume by less than a factor of 2. There is at most only a slight increase in particle size.

D. Aerosol Mass and Chemical Composition. The results from collecting aerosol samples onto filter substrates are listed in Table 5. For the flash photolysis experiments, the raw mass, ranging from 0.1 to 2.6 mg, is converted into a mass concentration by normalizing for the number of laser pulses and for the irradiated volume of 93 cm^3. As the initial toluene level is varied by a factor of 7, there is less than a 40% variation in the aerosol mass concentration, which corroborates the aerosol volume measurements made with the SMPS (Table 3). Utilizing the assumption of 100 amu for the aerosol constituent compounds, the mass concentration is further converted into an effective gaseous molecular concentration of oxidation products that

TABLE 4: Aerosol Measurements: Flow Reactor

	experimental conditions (Torr)						SMPS measurements				model
variable	toluene	Cl_2	O_2	CH_3OH	NO	dilution ratio	(est) $[Cl]_0$ ($\times 10^{14}$/cm^3)	particle no. ($\times 10^6$/cm^3)	particle volume ($\times 10^{11}$ nm^3/cm^3)	dia (nm)	[Criegee] ($\times 10^{11}$/cm^3)
$C_6H_5CH_3$	0.13	0.79	59			40	1.8	79	15	30	38
	0.33	0.79	59			40	1.8	45	21	39	14
	0.66	0.79	59			40	1.8	17	21	53	6.1
	1.3	0.79	59			40	1.8	3.5	21	90	2.4
	2.6	0.79	59			40	1.8	0.47	17	164	0.8
Cl_2	1.3	0.39	60			36	1.3	0.027	0.57	134	0.8
	1.3	0.59	60			36	1.9	1.3	17	113	2.0
	1.3	0.79	60			36	2.5	4.7	25	83	3.3
	1.3	1.18	60			36	3.8	19	38	59	7.1
	1.3	1.57	60			36	5.1	39	49	51	13
HO_2	1.29	0.6	58	0		20	1.4	0.2	1.5	105	1.5
	1.29	0.76	58	0.34		20	1.7	0.06	0.55	105	1.3
	1.25	0.7	58	0		19	1.6	0.19	0.8	100	2.0
	1.25	0.93	58	0.49		19	2.1	0.026	0.17	100	1.7
	1.26	0.6	57	0		20	1.4	0.13	0.9	110	1.5
	1.26	0.91	57	0.66		20	2.1	0.002	0.016	100	1.3
NO	2.65	0.79	58		0	36	1.8	0.03	1.1	190	0.78
	2.65	0.79	58		0.0021	36	1.8	0.007	0.08	120	0.78
	2.65	0.79	58		0.0042	36	1.8	0.002	0.007	88	0.78
	2.65	0.79	58		0.021	36	1.8	0	0		0.78
	2.65	0.79	58		0.104	36	1.8	0	0		0.77
	0.33	0.79	58		0	36	1.8	1.8	4.9	40	14
	0.33	0.79	58		0.0021	36	1.8	0.3	0.16	54	14

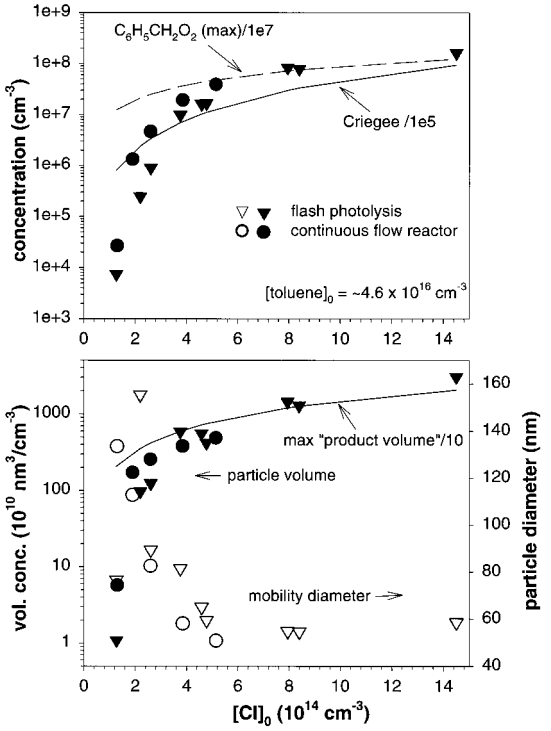

Figure 5. Aerosol characteristics as a function of initial chlorine atom concentration. (Top) Measured particle number (symbols) and model calculations of peak benzylperoxy radical and Criegee intermediate concentrations (lines). (Bottom) Measured particle volume concentration (filled symbols) and geometric mean diameter (open symbols) and calculated maximum "product volume" (line). Flash photolysis data are from Table 3 ($[Cl]_0$ varied); continuous flow data, at $t = 2$ s, are from Table 4 ($[Cl_2]_0$ varied).

ended up in the aerosol phase. The results indicate an effective concentration of $\sim 1 \times 10^{14}$ molecules/cm^3, or about 25% of the initial radical concentration. This is 2−3 times more aerosol product than indicated by the SMPS measurements. One explanation for the discrepancy could be the difficulties mentioned in section IIC regarding the CPC and molecular chlorine; however, even the most careful of these experiments did not yield a higher than ~10% conversion to aerosol. Another possibility is that gaseous compounds were collected onto the filters in addition to the aerosol particles. Although control experiments showed that toluene, benzaldehyde, and benzyl alcohol are not trapped by the filters, it is possible that other gaseous oxidation products do adsorb onto the filters, or that they, and possibly toluene, benzaldehyde, and benzyl alcohol, adsorb onto or react with the aerosol particles that have been trapped by the filter.

A typical chromatogram of the extract from particulate matter collected onto filter substrates is shown in Figure 10A. The two major components, benzaldehyde and benzyl alcohol, are positively identified by comparison to the respective reference compounds. These two components, plus the tentatively assigned benzyl hydroperoxide, comprise ~23% of the mass collected by the filters. As with the total mass, the concentrations of these species are insensitive to the variation in initial toluene level. It is interesting, however, that benzaldehyde and benzyl alcohol are found in nearly equal amounts in the aerosol, whereas the oxidation chemistry yields via reactions 4 and 5 a 3:1 benzaldehyde to benzyl alcohol ratio. Figure 10B shows the chromatogram plotted in terms of the intensity of the mass 91 benzyl fragment, which, aside from benzyl alcohol and benzyl chloride, is dominated by the aerosol components eluting between 900 and 1200 s. Compounds eluting between 400 and 800 s do not exhibit a benzyl fragment, but largely do contain the mass 77 phenyl fragment.

E. Effects of NO and HO_2. Both NO and HO_2 react rapidly with benzylperoxy radicals and compete with this radical's self-reaction. Since this competition alters the primary toluene oxidation pathway, it is instructive to examine how these reactants affect aerosol formation. The reaction between $C_6H_5CH_2O_2$ and HO_2 is expected to proceed primarily via reaction 7 to form benzyl hydroperoxide.[21] Even in the absence of the methanol precursor, HO_2 is formed as a secondary toluene oxidation product by the $C_6H_5CH_2O + O_2$ reaction. The primary implications of cogenerating HO_2 , therefore, are to increase its presence, and to introduce it earlier in the oxidation pathway. This leads to a higher yield of the benzyl hydroperoxide product

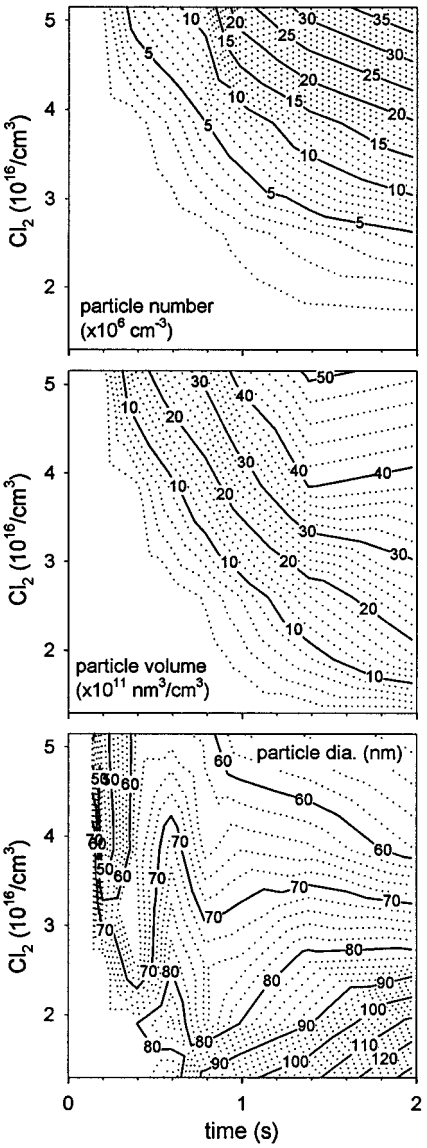

Figure 6. Aerosol time evolution as a function of initial radical concentration (based on $[Cl_2]_0$): (top) particle number; (middle) particle volume; (bottom) particle diameter. Reaction conditions are listed in Table 4 ($[Cl_2]$ varied).

at the expense of benzaldehyde and benzyl alcohol. However, since reaction 7 is a radical termination step, another important effect is that the added HO_2 leads to a more rapid loss of radicals from the reaction mixture, thereby potentially inhibiting the formation of the critical nuclei.

The data in Tables 3 and 4 show that, as the amount of added HO_2 approaches the initial $C_6H_5CH_2O_2$ concentration, there is a $1-2$ order of magnitude decrease in the particle number concentration. The aerosol volume also decreases as additional HO_2 is introduced into the reaction mixture. In the flow reactor experiments, the particle diameter remains at $\sim$105 nm; thus, the volume decrease simply mimics the decline in particle number. In the flash photolysis experiments the particle diameter increases to about 160 nm with added HO_2, partially offsetting the decline in particle number. This difference in behavior possibly originates from the 2.5 times higher initial radical concentrations used in the flash photolysis experiments.

Figure 11 displays the effect of NO on the aerosol number and volume concentrations. The number of particles experiences a nearly exponential decline as a function of added NO, falling

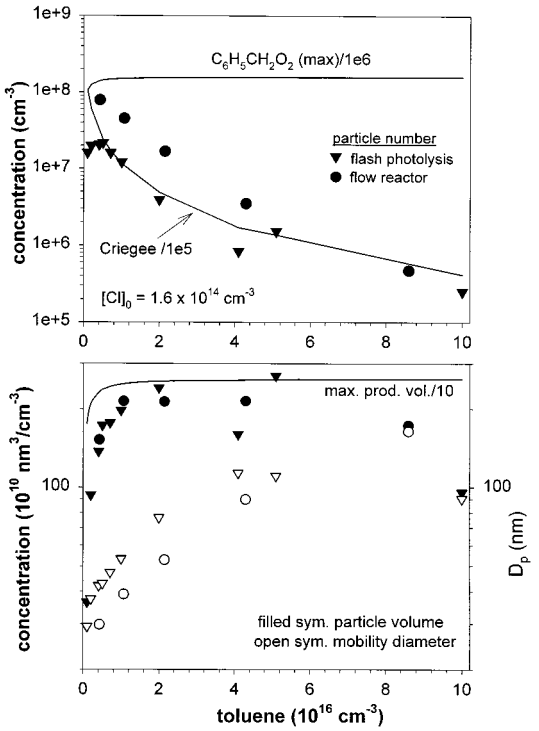

Figure 7. Aerosol characteristics as a function of initial toluene concentration. (Top) Measured particle number (symbols) and model calculations of peak benzylperoxy radical and Criegee intermediate concentrations (lines). (Bottom) Measured particle volume concentration and geometric mean diameter (symbols) and calculated maximum "product volume" (line). Data, at $t = 2$ s, are from Tables 3 and 4 ($[\text{toluene}]_0$ varied).

about 3 orders of magnitude as the NO level is raised over the $(0-1) \times 10^{16}$ cm^{-3} range. Even in the presence of NO, decreasing the amount of toluene increases the particle number concentration (Table 4). The NO has little effect on the mean particle diameter, which exhibits only a small decline, from about 75 to 65 nm, over the range of NO explored. Therefore, the aerosol volume dependence on NO essentially mirrors the decrease in particle number.

Since the rate constant for the $C_6H_5CH_2O_2 + NO$ reaction is about 4 times faster than for the benzylperoxy self-reaction (Table 2), even a small amount of NO will change the distribution of primary oxidation products. With no added NO, reactions 4 and 5 imply a 3:1 ratio of benzaldehyde to benzyl alcohol. Adding NO increases this ratio, because reactions 6 and 5 lead solely to the benzaldehyde product. When the NO level becomes comparable to, or exceeds that of, benzylperoxy, there is sufficient NO for the production of benzyl nitrite, via

$$C_6H_5CH_2O + NO \rightarrow C_6H_5CH_2ONO \qquad (8)$$

to become important. As the NO level is raised further, the nitrite will supplant benzaldehyde as the major oxidation product.

These changes in oxidation product distribution are consistent with the decrease in aerosol mass collected onto filters and the changes in chemical composition listed in Table 5. The aerosol mass concentration per photolysis pulse falls by a factor of $\sim$10 as NO is increased from 0×10^{15} to 4×10^{15} cm^{-3}, or a factor of $\sim$5 for a $(0-3) \times 10^{15}$ cm^{-3} change in NO, in agreement with the decrease in aerosol volume shown in Figure 11. However, the mass decreases in benzaldehyde and benzyl alcohol components are approximately 2 times greater. There is an increase in the tentatively assigned benzyl nitrite compo-

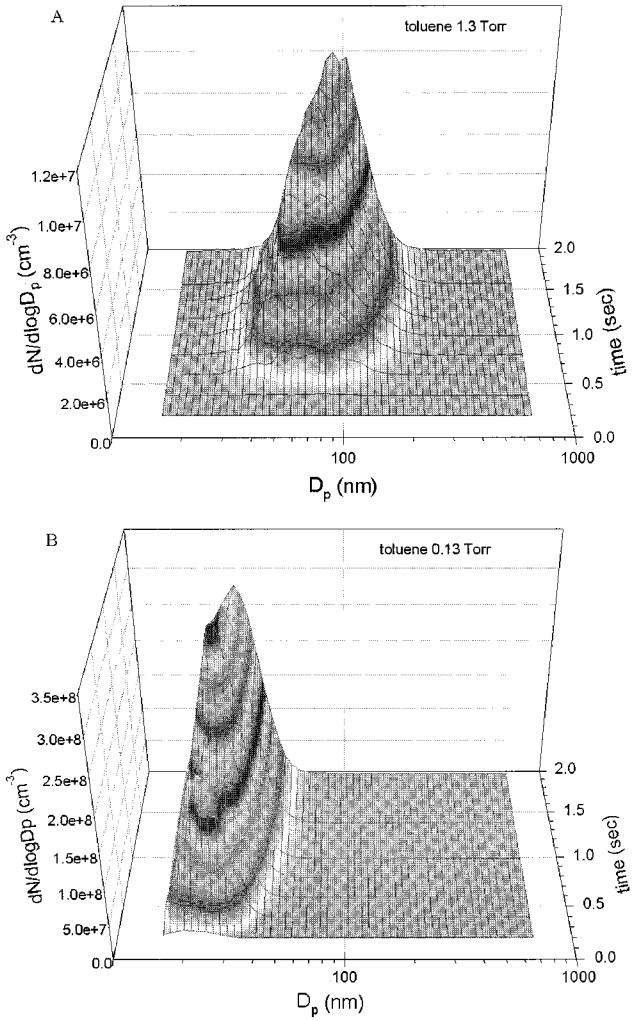

Figure 8. Time evolution of aerosol size distribution for initial toluene concentrations of 1.3 Torr (A) and 0.13 Torr (B).

nent, as well as other unidentified components, as indicated by the fact that a progressively smaller fraction of the aerosol mass is attributable to the listed species.

V. Discussion

It is useful to summarize the salient features of the aerosol formation measurements described above. The time evolution occurs in three phases: an incubation period, rapid growth in particle number and aerosol volume at a diameter that is near fully grown, and a plateau region during which the particles in some cases exhibit slow secondary growth. Increasing the initial radical concentration leads to a shorter incubation time, larger particle number and aerosol volume, smaller particle diameter, and less secondary growth. Increasing the initial toluene level results in a longer incubation period, lower particle number, larger mean diameter, and more secondary growth. Particle volume is comparatively unaffected by toluene concentration. The addition of either NO or HO_2 suppresses both particle number and aerosol volume.

The three phases of aerosol evolution evident in Figures 6, 8, and 9 can be associated with the gas phase oxidation chemistry that produces semivolatile products, the nucleation of these species as they reach supersaturation, and the growth of the critical nuclei. In classical nucleation theory, which applies to stable supersaturated vapors (or mixtures), the nucleation rate is derived from consideration of the free energy of formation

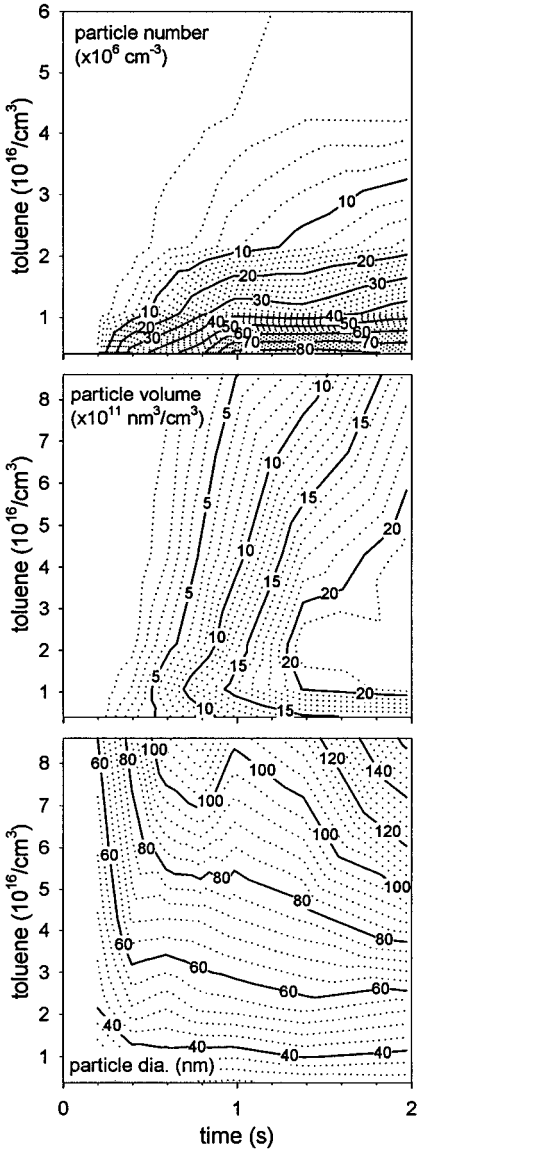

Figure 9. Aerosol evolution as a function of toluene concentration: (top) particle number; (middle) particle volume; (bottom) particle diameter. Reaction conditions are listed in Table 4 ($[C_6H_5CH_3]$ varied).

for critical clusters (ΔG^*)[36]

$$J = K \exp(-\Delta G^*/kT)$$

$$J = \left(\frac{2\sigma}{m\pi}\right)^{1/2} \frac{n^2 v}{S} \exp\left(\frac{-16\pi v^2 \sigma^3}{3(kT)^3(\ln S)^2}\right) \qquad (9)$$

and is expressed in terms of the supersaturation $S = P/P_e$, and physical properties of the bulk liquid. Here m is the mass of the vapor phase molecules, n is their concentration, v is the molecular volume, and σ is the surface tension. In a qualitative sense, the variations in aerosol formation with changes in initial radical concentration follow eq 9; increasing $[Cl]_0$ leads to higher concentrations (supersaturations) of toluene oxidation products and this, in turn, leads to higher nucleation rates and greater particle concentrations. However, a more quantitative application of eq 9 is at present untenable for two reasons: (1) the nucleating species have not been identified and (2) it is not evident that there is a clear separation between the time scale of the gas phase chemistry leading to semivolatile products and the time scale of their subsequent nucleation. That is, the observed

TABLE 5: Particulate Mass and Composition

variable	$[Cl]_0$ (10^{14} cm^{-3})	toluene (10^{16} cm^{-3})	NO or CH_3OH (10^{14} cm^{-3})	filter mass (μg)	mass conc per pulse[a] (ng/cm^3)	eff no. conc[b] (10^{14} cm^{-3})	RCH_3[c] (ng/cm^3)	RCHO[c] (ng/cm^3)	RCH_2OH[c] (ng/cm^3)	RCH_2OOH (tent.) (ng/cm^3)	RCH_2ONO (tent.) (ng/cm^3)	identified/ filter mass
toluene	4.2	1.0		370	11	0.67	0	1.2	1.1	0.06		0.21
	4.2	4.9		650	19	1.2	0	2.5	2.3	0.15		0.26
	3.9	1.0		820	16	1.0	0	1.7	1.7	0.09		0.22
	3.9	4.9		940	19	1.1	0	2.0	1.9	0.09		0.22
	3.7	7.3		840	17	1.0	0	1.8	1.7	0.10		0.21
NO	3.9	4.9	0	940	19	1.1	0	2.0	1.9	0.09	0.00	0.22
	3.5	4.9	6	400	8.0	0.48	0.14	0.45	0.35	0.04	0.11	0.15
	3.2	4.9	25	220	4.4	0.26	0.06	0.19	0.15	0.02	0.06	0.11
	2.9	4.9	40	100	2.0	0.12	0.00	0.07	0.04	0.01	0.01	0.06
	4.2	4.9	0	1830	23	1.4	0.00	1.5	1.6	0.14	0.00	0.14
	4.0	4.9	8	1180	15	0.91	0.21	0.49	0.47	0.06	0.11	0.11
	4.4	4.9	17	930	12	0.73	0.16	0.30	0.26	0.04	0.08	0.08
	4.2	4.9	32	390	5.0	0.30	0.07	0.17	0.16	0.02	0.04	0.10
HO_2	5.3	4.8	1.7	380	7.6	0.46	0	0.73	0.79	0.06		0.21
	3.7	4.8	0	960	19	1.2	0	1.9	2.2	0.15		0.23
HO_2	2.1	4.1	0.49	550	0.43	0.026	0	0.045	0.046	0.005		0.22
flow reactor	2.1	4.1	0	2620	1.8	0.11	0	0.13	0.15	0.013		0.16

[a] Mass conc = filter mass/no. of laser pulses/irradiated volume. [b] Eff no. conc = mass concentrated/mass per molecule, assuming a generic molecular weight of 100 amu for the molecules comprising the aerosol. [c] R = C_6H_5.

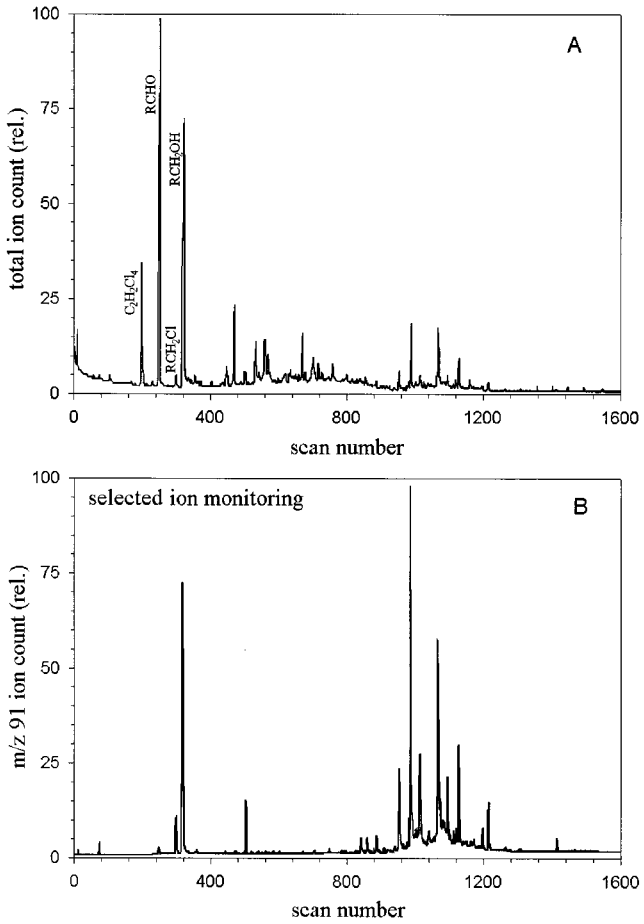

Figure 10. Gas chromatogram of aerosol particulate matter extracted with methylene chloride: (A) based on total ion count; (B) based on ion count of 91 amu peak in mass spectrum.

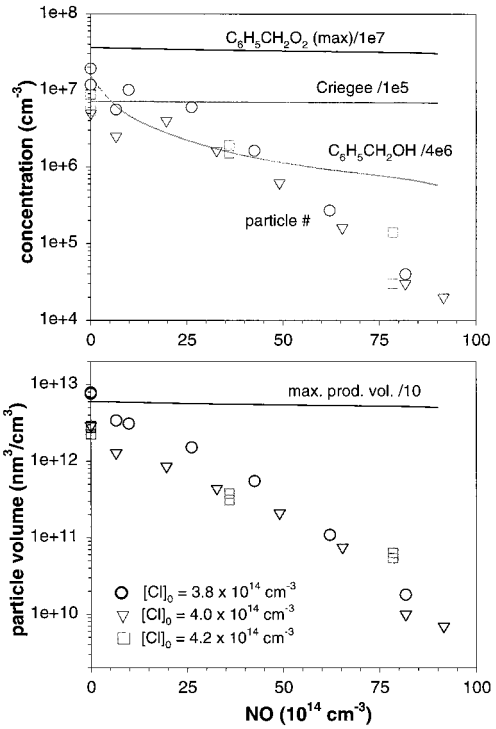

Figure 11. Aerosol characteristics as a function of added NO concentration: (top) measured particle number (symbols) and model calculations of peak benzylperoxy radical, Criegee intermediate, and benzyl alcohol concentrations (lines); (bottom) measured particle volume concentration (symbols) and calculated maximum "product volume" (line). Data and reactant concentrations are listed in Table 4 (NO varied).

incubation times could arise from the gas phase oxidation chemistry, the nucleation dynamics, or both.

Let us examine the aerosol dynamics from a somewhat different viewpoint. Assume that some combination of semivolatile products produces critical nuclei. These then evolve to the observed particle number and aerosol volume concentrations by a combination of coagulation and condensation/adsorption. Let us suppose first that coagulation is the dominant process, but that for some reason we do not observe the small particles, rather only the nearly fully grown ones. Since the mean free path at the 1 atm pressure and 295 K temperature of these experiments is 65 nm, the coagulation occurs primarily in the free molecule regime; thus, the coagulation rate constant, approximated as the collision of two identical diameter spheres, is

$$k_{\text{coagul}} = \sigma\langle v_{\text{rel}}\rangle = (96kTD_p/\rho)^{1/2}$$

where D_p is the particle diameter and ρ is its density. At a constant aerosol volume concentration of V_A, the number concentration of particles, all assumed to have diameter D_p, is

[particle] $= 6V_A/\pi D_p^3$. Thus, in this simplified treatment, as the particles grow by coagulation, their collision frequency falls as

$$Z = \frac{6V_A}{\pi}\left(\frac{96kT}{\rho}\right)^{1/2} D_p^{-5/2} \qquad (10)$$

At $V_A = 5 \times 10^{12}$ nm^3/cm^3, near the high end of the aerosol volumes recorded in the present experiments, the collision frequency drops to 1 s^{-1} when the particle diameter reaches about 30 nm. Under a more moderate aerosol volume of 1×10^{12} nm^3/cm^3, the 1 s^{-1} collision frequency is reached at a particle diameter below 20 nm. The implication is that for the aerosol volume concentrations recorded in this study, particle growth by coagulation "freezes out" for particles larger than the 15−30 nm range, well short of the ∼70 nm nascent mean particle diameters that we typically observe.

Suppose instead that the critical nuclei, perhaps after an initial period of coagulation, grow primarily by condensation/adsorption. Staying in the free molecule regime, the rate constant is well approximated as

$$k_{cond} = (\pi/4)D_p^2\langle v_{molec}\rangle$$

where the collision cross section is dominated by the particle diameter and the relative velocity is dictated by the gaseous molecular motion. From this, the particle's diameter growth rate becomes

$$dD_p/dt = mN_{molec}\langle v_{molec}\rangle/2\rho \qquad (11)$$

where m is the mass per molecule, N_{molec} is the concentration of condensable species, and ρ is the particle's density. The rate of change in diameter is independent of particle size. The average speed of our assumed 100 amu "generic" oxidation product is $\langle v_{molec}\rangle = 2.5 \times 10^4$ cm/s at 295 K. Assuming further that 10% of the oxidation products are condensable (from a total product concentration of typically 4×10^{14} molecules/cm^{-3}), the diameter growth rate is approximately 830 nm/s. Consequently, less than 0.1 s (the approximate time resolution of the flow reactor) is needed to grow the nuclei to the 70 nm diameter range at which particles are typically first observed. As the particle diameters surpass the 65 nm mean free path, the condensation dynamics enters the transition regime between molecular and diffusion-limited transport, and the particle growth rate will slow as the vapor in the vicinity of the particles is depleted.

The above analysis suggests that formation of the nuclei, due either to gas phase chemistry or to the nucleation process, presents the rate-limiting step in the aerosol evolution. Once formed, the nuclei rapidly (on our observational time scale of ∼0.1 s) grow to a size dictated by the number of nuclei formed and by the amount of available condensable material. This explains, for example in Figure 8A, why there is a rapid increase in particle number between ∼0.5 and 1.0 s, but the particle mean diameter remains constant at ∼70 nm.

Under conditions where high aerosol volumes are produced, $V_A > \sim 4 \times 10^{12}$ nm^3/cm^3, coagulation will continue to be competitive over the 0.1 s time scale for particles up to ∼10 nm in diameter, and, therefore, will limit particle number. This is illustrated by the leveling off of the particle number concentration as a function of $[Cl]_0$ above a value of $[Cl]_0 \cong 4 \times 10^{14}$ cm^{-3} in Figure 5. The additional slow secondary growth at a rate of about 20 nm/s during the 1.0−2.0 s period (see Figure 8A) occurs either from the adsorption of minor oxidation

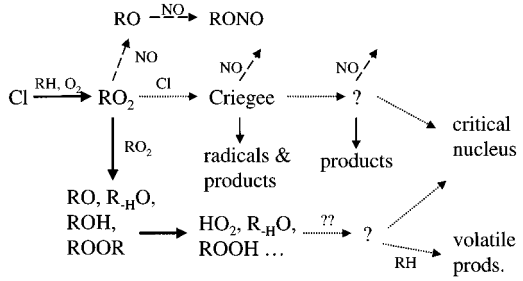

Figure 12. Postulated mechanism for aerosol formation from the Cl-initiated oxidation of toluene (R = C_6H_5).

products that are present in small concentrations (from eq 11, the concentration required for a growth of 20 nm/s is $N_{molec} \cong 1 \times 10^{12}$ cm^{-3}, assuming a sticking coefficient of unity), or from the adsorption and dissolution of major species that are present at levels below supersaturation.

The latter possibility is consistent with our observations that, although neither of the principal oxidation products, benzaldehyde or benzyl alcohol, is formed in quantities above their saturation vapor pressure, they are both nonetheless found in the filter collected aerosol particles. For an initial radical concentration of $[Cl]_0 = 4 \times 10^{14}$ cm^{-3}, their concentrations are 1.8×10^{14} cm^{-3} and 0.6×10^{14} cm^{-3}, well shy of their respective vapor pressures of 2.4×10^{16} and 2.5×10^{15} cm^{-3} at 20 °C.[37] The presence of these species in the aerosol particles suggests that they are incorporated into the aerosol via adsorption and possibly dissolution.

Thus far, the aerosol dynamics described above explains the changes in aerosol properties and evolution that arise from variations in $[Cl]_0$ and from the addition of NO and HO_2 , assuming that the latter interfere with aerosol formation by reacting with the benzylperoxy radicals and, thereby, altering the nature of the oxidation products. However, it does not explain the sensitive dependence of aerosol formation on changes in initial toluene level. As shown in the top panel of Figure 7, the concentration of benzylperoxy radicals is nearly independent of $[C_6H_5CH_3]_0$ over the same range that the particle number concentration falls by 3 orders of magnitude. Likewise the levels of principal oxidation products (benzaldehyde and benzyl alcohol) are insensitive to changes over this toluene concentration range.

It is difficult to explain the influence that toluene has on the aerosol evolution. To first order, it should not have one. Given that it does, one would expect added toluene to increase particle formation, for example by secondary reactions with the radicals that are photolytically produced, but not to decrease it. Furthermore, to the extent that such secondary chemistry alters the amounts and natures of supersaturated oxidation products, changing the toluene concentration should affect both particle number and aerosol volume, and not just the former. For example, one might surmise that a minor reaction where Cl atoms attack the aromatic ring of toluene increases the amount of supersaturated vapors, but this should produce both higher aerosol number and volume concentrations.[15]

We suggest that distinct chemical pathways, as illustrated in Figure 12, are responsible for producing the critical nuclei versus supplying the semivolatile material for particle growth. A secondary reaction between chlorine atoms and benzylperoxy radicals

$$C_6H_5CH_2O_2 + Cl \rightarrow C_6H_5CHOO + HCl \qquad (12)$$

is hypothesized to generate (probably after significant additional

chemistry) the critical nuclei, whereas the major oxidation pathway yields the condensable species (for example the ~20% of the aerosol volume identified as benzaldehyde and benzyl alcohol). The reactions of chlorine atoms with peroxy radicals are known to be very fast, and have been previously postulated to proceed in part (~50% yield) via the Criegee intermediate,[38] a biradical that is usually associated with the ozonolysis of alkenes.[39−41]

This model explains both the inverse dependence of particle number density on $[C_6H_5CH_3]_0$ and the lack of an aerosol volume dependence. Under high toluene concentrations, the photolyzed chlorine atoms are immediately consumed by reaction with toluene. As the toluene level decreases, the Cl lifetime lengthens, thereby increasing the probability of reaction between chlorine atoms and benzylperoxy radicals. This raises the fraction of radicals proceeding via the Criegee intermediate, as indicated in the top panel of Figure 7. Qualitatively, the modeled Criegee concentration mimics that of particle number. Its quadratic dependence on $[C_6H_5CH_3]_0$ is shallower than that of particle number, but this is likely because nucleation of the products from the Criegee intermediate remains a nonlinear function of their concentration (as in eq 9). Although it is a minor channel, approximately $10^{11}-10^{13}$ Criegee intermediates/cm^3 are produced over the range of toluene concentration explored. This is more than sufficient to nucleate the observed 10^5-10^8 particles/cm^3; but since it represents 0.02%−2% of the reaction products, the Criegee pathway is insufficient to account for the total aerosol volume. Because the growth of these nuclei occurs primarily by the condensation/adsorption of compounds produced by the major oxidation pathway, and since these product concentrations are little affected by the variation of $[C_6H_5CH_3]_0$, aerosol volume remains nearly independent of toluene level. The net amount of condensable material, approximately 10% of the oxidation products, finds fewer nuclei as $[C_6H_5CH_3]_0$ decreases; thus, the mean particle diameter increases with increasing toluene concentration, as observed in the data.

One might counter that toluene could similarly compete with a different secondary Cl reaction rather than the one with benzylperoxy radical (reaction 12). However, model calculations based in Table 1 show that a secondary reaction between Cl and benzaldehyde, the most prevalent product, would net at most $\sim 10^6-10^9$ product molecules/cm^3, an unlikely number to yield 10^5-10^8 particles/cm^3. We cannot conclusively rule out that toluene does not inhibit some other minor reaction channel that occurs further down the principal oxidation pathway and, therefore, indicate this possibility on the model in Figure 12. However, the Cl reaction with $C_6H_5CH_2O_2$ deserves consideration since it explains the data and there is precedence for its occurrence. It is also a highly energetic species that could lead to ring opening products analogous to those from the OH attack of toluene, which leads to aerosol formation under atmospheric conditions.

VI. Conclusions

The primary gas phase pathways for the Cl-initiated oxidation of toluene are quite analogous to those of other substituted methanes. This occurs because of the high propensity for chlorine atoms to abstract a methyl hydrogen as opposed to attacking the aromatic ring. Thus, the phenyl group acts essentially as a bystander, and we find in agreement with previous studies that the principal degradation products are benzaldehyde and benzyl alcohol and that they appear in a 3:1 ratio.[17,21] Our measurement of $k_4 = (8 \pm 2) \times 10^{-12}$ cm^3 s^{-1} for the benzylperoxy self-reaction is in excellent agreement with the single available literature value.[21] In its reactions with NO and HO_2, the benzylperoxy radical again behaves like a substituted methylperoxy radical. Both reactions are fast and typical of their class: $k_6 = (2.7 \pm 0.5) \times 10^{-11}$ cm^3 s^{-1} and $k_7 = (1.0 \pm 0.2) \times 10^{-11}$ cm^3 s^{-1} (ref 21).

The nonlinear increases in particle number and aerosol volume that occur as the initial radical concentration is raised, are consistent with the oxidation chemistry producing semivolatile species that grow in concentration to supersaturation and subsequently nucleate. Considerations of the net aerosol volume lead to the conclusion that beyond about 10−30 nm, particle growth is dominated by condensation/adsorption, and that these processes contribute the bulk of the aerosol volume. The suppression of aerosol formation by the addition of NO or HO_2 indicates the importance of the benzylperoxy radical as an intermediate leading to the aerosol. Both species serve to scavenge the benzylperoxy radical and act as radical termination steps. NO limits the benzaldhyde and benzyl alcohol yields, leading instead to benzyl nitrite. Similarly HO_2 alters the product distribution by producing benzyl hydroperoxide.

The essentially orthogonal dependencies of particle number versus aerosol volume on the initial toluene concentration and the time dependence of the aerosol evolution require this model to be modified. Particle number is relatively insensitive to time, yet it decreases dramatically with increasing toluene level. In contrast, aerosol volume is comparatively insensitive to toluene level, but increases with time. These observations suggest that separate chemical pathways are responsible for creating the species that nucleates, as opposed to those forming the bulk of the particle volume. We propose that a reaction between chlorine atoms and benzylperoxy radicals to form a Criegee intermediate is the key step for determining particle number; however, the evidence at this time is not conclusive. The proposed mechanism, though, explains the contrasting behavior of particle number and aerosol volume with respect to initial toluene level, as well as the observed changes in particle diameter.

Acknowledgment. We appreciate a number of insightful conversations with Steve Harris over some of the fine points in aerosol growth by coagulation and condensation, as well as the discussions with Mike Hurley and Lena Christensen about their smog chamber experiments. Rune Karlsson's part of the research was partly made possible by grants from the Sweden-America Foundation, the Swedish Institute, Preem's Environmental Foundation, and the Swedish Association of Graduate Engineers.

References and Notes

(1) Pope, C. A., III; Bates, D. V.; Raizenne, M. E. *Environ. Health Perspect.* **1995** *103*, 472.
(2) Schwartz, J.; Dockery, D. W.; Neas, L. M. *J. Air Waste Manage. Assoc.* **1996**, *46*, 927.
(3) "National Ambient Air Quality Standard for Particulate Matter: Final Rule", *Federal Register* **1997**, *62*, 38652.
(4) Grosjean, D.; Friedlander, S. K. *J. Air Pollut. Control Assoc.* **1975**, *25*, 1038.
(5) Gartrell, G., Jr.; Friedlander, S. K. *Atmos. Environ.* **1975**, *9*, 279.
(6) Turpin, B. J.; Huntzicker, J. J. *Atmos. Environ.* **1995**, *29*, 3527.
(7) Griffen, R. J.; Cocker, D. R., III; Flagan, R. C.; Seinfeld, J. H. *J. Geophys. Res.* **1999**, *104*, 3555.
(8) Odum, J. R.; Jungkamp, T. P. W.; Griffin, R. J.; Forstner, H. J. L.; Flagan, R. C.; Seinfeld, J. H. *Environ. Sci. Technol.* **1997**, *31*, 1890.
(9) Leach, K. B.; Kamens, R. M.; Strommen, M. R.; Jang, M. *J. Atmos. Chem.* **1999**, *33*, 241.
(10) Liang, C.; Pankow, J. F.; Odum, J. R.; Seinfeld, J. H. *Environ. Sci. Technol.* **1997**, *31*, 3086.
(11) Odum. J. R.; Hoffman, T.; Bowman, F.; Collins, D.; Flagan, R. C.; Seinfeld, J. H. *Environ. Sci. Technol.* **1996**, *30*, 2580.
(12) Pankow, J. F. *Atmos. Environ.* **1994**, *28A*, 185.

(13) Bowman, F. M.; Odum, J. R.; Seinfeld, J. H.; Pandis, S. N. *Atmos. Environ.* **1997**, *31*, 3921.
(14) Yu, J.; Flagan, R. C.; Seinfeld, J. H. *Environ. Sci. Technol.* **1998**, *32*, 2357.
(15) Odum, J. R.; Jungkamp, T. P. W.; Griffin, R. J.; Flagan, R. C.; Seinfeld, J. H. *Science* **1997**, *276*, 96.
(16) Barrie, L. A.; den Hartog, G.; Bottenheim, J. W. *J. Atmos. Chem.* **1989**, *9*, 101.
(17) Seuwen, R.; Warneck, P. *Int. J. Chem. Kinet.* **1995**, *28*, 315.
(18) Maricq, M. M.; Wallington, T. J. *J. Phys. Chem.* **1992**, *96*, 986.
(19) Maricq, M. M.; Szente, J. J. *J. Phys. Chem.* **1996**, *100*, 4507.
(20) Maricq, M. M.; Szente, J. J.; Hybl, J. D. *J. Phys. Chem.* **1997**, *101*, 5155.
(21) Nozière, B.; Lesclaux, R.; Hurley, M. D.; Dearth, M. A.; Wallington, T. J. *J. Phys. Chem.* **1994**, *98*, 2864.
(22) Maricq, M. M.; Szente, J. J. *J. Phys. Chem.* **1994**, *98*, 2078.
(23) Willeke, K.; Baron, P. A. Eds., *Aerosol Measurement, Principles, Techniques, and Applications*; Van Nostrand Reinhold: New York, 1993.
(24) Tsang, W.; Hampson, R. F. *J. Phys. Chem. Ref. Data* **1986** *15*, 1087.
(25) Fenter, F. F.; Noziere, B.; Caralp, F.; Lesclaux, R. *Int. J. Chem. Kinet.* **1994**, *26*, 171.
(26) Benson, S. W.; Weissman, M. *Int. J. Chem. Kinet.* **1982**, *14*, 1287.
(27) Nelson, H. H.; McDonald, J. R. *J. Phys. Chem.* **1982**, *86*, 1242.
(28) Muller-Markgraf, W.; Troe, J. *J. Phys. Chem.* **1988**, *92*, 4899.
(29) DeMore, W. B.; Sander, S. P.; Golden, D. M.; Hampson, R. F.; Kurylo, M. J.; Howard, C. J.; Ravishankara, A. R.; Kolb, C. E.; Molina, M. J. Chemical kinetics and photochemical data for use in stratospheric modeling. Evaluation No. 12; JPL Publication 97-4, 1997; pp 1-266.
(30) Biggs, P.; Canosa-Mas, C. E.; Fracheboud, J.-M.; Shallcross, D. E.; Wayne, R. P. *J. Chem. Soc., Faraday Trans.* **1997**, *93*, 2481.
(31) Heicklen, J. *Adv. Photochem.* **1988**, *14*, 177.
(32) Tyndall, G. S.; Wallington, T. J.; Hurley, M. D.; Schneider, W. F. *J. Phys. Chem.* **1993**, *97*, 1576.
(33) Meier, U.; Grotheer, H. H.; Riekert, G.; Just, Th. *Ber. Bunsen-Ges. Phys. Chem.* **1985**, *89*, 325.
(34) Ebata, T.; Obi, K.; Tanaka, I. *Chem. Phys. Lett.* **1981**, *77*, 480.
(35) Lightfoot, P. D.; Cox, R. A.; Crowley, J. N.; Destriau, M.; Hayman, G. D.; Jenkin, M. E.; Moorgat, G. K.; Zabel, F. *Atmos. Environ.* **1992**, *26A*, 1805.
(36) Oxtoby, D. W. *J. Phys.: Condens. Matter*, **1992**, *4*, 7627.
(37) Handbook of Chemistry and Physics, 61st ed.; Weast, R. C., Ed.; CRC Press: Boca Raton, FL, 1981; p D-219.
(38) Maricq, M. M.; Szente, J. J.; Kaiser, E. W.; Shi, J. *J. Phys. Chem.* **1994**, *98*, 2083.
(39) Criegee, R. *Rec. Chem. Prog.* **1957**, *18*, 111.
(40) Niki, H.; Maker, P. D.; Savage, C. M.; Breitenbach, L. P. *Chem. Phys. Lett.* **1977**, *46*, 327.
(41) Atkinson, R.; Tuazon, E. C.; Aschmann, S. M. *Environ. Sci. Technol.* **1995**, *29*, 1860.